Technical sciences

UDC 678.027.76

Morozov Kyrylo

Mining Equipment Specialist

Donbas State Technical University

ORCID: 0009-0009-5565-8452

DOI: https://doi.org/10.25313/2520-2057-2026-11-15105

WALL-GRADIENT EQUILIBRATION PROTOCOL FOR LINEAR REHEAT STRETCH BLOW MOLDING OF LARGE-FORMAT PET CONTAINERS

Summary. *Large-format polyethylene terephthalate (PET) containers above five gallons require preforms exceeding three hundred grams and five millimeters in wall thickness, conditions under which standard infrared heating produces strong radial temperature gradients, outer-skin crystallization, and asymmetric biaxial orientation during stretching on linear equipment. Published process literature has concentrated on rotary stretch-blow systems and beverage formats below three liters, leaving the thick-preform linear regime fragmentarily described. This article presents and validates the Wall-Gradient Equilibration Protocol (WGEP), an engineering methodology that couples zoned radiative-convective heating with adaptive pre-blow timing on a linear stretch-blow line. Implementation took place over twenty-four weeks at a Ring Container Technologies plant in South Carolina on a six-cavity SIPA SFL Series machine producing 18.9-liter food-grade PET containers from 340-gram preforms. Measurement combined offline-calibrated thermocouple mapping in a laboratory rig with production-line infrared pyrometry, FLIR thermal imaging, and post-*

blow ultrasonic profilometry. Through-thickness temperature gradient declined from 16.5 °C to 4.2 °C, wall-thickness standard deviation fell by thirty-three percent, Top Load resistance per ASTM D2659 rose from 168 to 196 kilograms, burst pressure improved by fifteen percent, and the rejection rate decreased from 1.4 to 0.5 percent across a fourteen-day production window. To the author's knowledge, no prior peer-reviewed work has reported integration of through-thickness gradient measurement with adaptive pre-blow control on linear stretch-blow equipment for heavy-preform large-format PET.

Key words: *reheat stretch blow molding, linear stretch-blow equipment, thick-wall PET preform, through-thickness temperature gradient, adaptive pre-blow timing, large-format container, Top Load resistance.*

Introduction. Polyethylene terephthalate (PET) has become the dominant polymer for many industrial container applications in the United States during the past two decades, particularly where weight advantage, clarity, gas-barrier characteristics, and food-grade recyclability are required [1]. Large-format containers, defined here as units between five and thirty liters intended for institutional food service, bulk water distribution, and industrial chemical packaging, have expanded at a different pace than the standard beverage segment because of demand from quick-service restaurant supply chains, food distribution networks, and household-cleaning product lines. Containers in this format typically weigh between one and two kilograms and require preforms between 300 and 700 grams, with wall thicknesses ranging from five to twelve millimeters before stretching.

Two stretch blow molding architectures dominate US PET production. Rotary systems such as the Sidel SBO series and Krones Contiform process beverage containers up to three liters at throughput rates above 16,000 units per hour and rely on short residence times in the infrared oven. Linear systems represented by SIPA SFL, KHS InnoPET Blomax, and Nissei ASB machines

operate at lower throughput but accommodate the thicker preforms required for containers above three liters [1]. Throughput is not the determining factor in this distinction. Heat penetration into a thick-walled semicrystalline polymer governs whether biaxial orientation occurs uniformly across the container wall, and linear ovens with longer residence times are the only practical option for preforms above 300 grams.

Temperature distribution through preform thickness during infrared reheat, crystallization kinetics, and biaxial deformation behavior have been studied extensively for standard fast-moving consumer goods geometries. Prior work has established that radial temperature profiles across thin preform walls under three millimeters govern bottle wall-thickness distribution and Top Load resistance [4], and that the temperature-dependent mechanical response of PET at industrial strain rates governs the uniformity of wall-thickness development during stretching [8]. Simulation models covering infrared absorption, non-isothermal viscoelastic behavior, and crystallization onset have been validated for preforms in the 0.5-to-3-liter range [1].

Existing literature contains two distinct gaps. Nearly all published process studies target preforms below 200 grams and walls under five millimeters, leaving the heavy-preform regime described mostly in industry technical bulletins and reference texts [1]. No peer-reviewed study has reported a measurement-driven process control strategy for managing through-thickness gradients in thick-wall preforms on linear stretch-blow equipment. Simulation studies by Lontos and Gregoriou addressed pre-blow timing for 1.5-liter geometries [11], and Salomeia, Menary, and Armstrong instrumented a stretch-blow machine for closed-loop process monitoring [12]; neither effort involved a measured wall-gradient signal coupled to pre-blow trigger logic on a multi-cavity linear machine producing heavy-format containers.

This article presents and validates an engineering protocol that bridges those gaps. The purpose of this study is to develop, implement, and validate a

measurement-driven heating and pre-blow control methodology for thick-wall preform processing on linear stretch-blow equipment. Wall-Gradient Equilibration Protocol (WGEP) integrates three components: modified oven zoning with convective stabilization gaps, a soak interval for radial heat diffusion, and gradient-triggered pre-blow sequencing on linear stretch-blow equipment. Four objectives organize the study. Specification of the heating sequence and stabilization-gap architecture that equalizes through-thickness temperature within four degrees Celsius before stretching forms the first. Coupling pre-blow timing to the measured gradient state forms the second. Quantification of the effect of the protocol on wall-thickness distribution, Top Load resistance, burst pressure, and rejection rate forms the third. Documentation of the trade-off between throughput penalty and quality gain completes the set, with results presented in a form usable by operators of comparable linear stretch-blow equipment.

Literature Review. Infrared heating of polyethylene terephthalate preforms operates on a semi-transparent absorption regime where the polymer transmits a substantial fraction of incident radiation in the near and mid-infrared bands, with absorption peaks near 3.3, 6.8, and 8.5 micrometers governing internal heat deposition. Monteix and coworkers built spectral absorption models from transmission and reflectance measurements on PET sheets ranging from 0.4 to 4 millimeters in thickness, demonstrating that thicker walls trap more energy near the outer surface and exhibit a strongly nonlinear radial temperature profile after passage through a lamp bank [2]. Cosson and colleagues advanced this analysis with a ray-tracing approach that captured internal reflections at the preform inner surface, predicting a secondary absorption peak roughly two thirds of the way through the wall thickness [5]. Saggin and coworkers established that non-contact temperature profiling using calibrated thermal imagers can resolve surface temperature with an uncertainty below 1.5 °C at production-line speeds, supporting inline gradient monitoring on industrial-scale systems [13]. Validity of the absorption-coefficient assumptions and surface-emissivity corrections used

in those studies has been demonstrated for wall thicknesses below four millimeters, with empirical confirmation at greater thicknesses still pending.

Stretch dynamics in injection stretch blow molding depend on a coupled response between strain rate, temperature, and the natural stretch ratio of PET, which is itself a function of crystallinity and molecular weight distribution [1]. Schmidt, Agassant, and Bellet developed an axisymmetric finite-element model that resolved the time evolution of bottle wall thickness during contact with the cavity surface, finding strong sensitivity to the pre-blow pressure profile [3]. In a parallel experimental investigation, Menary and colleagues conducted biaxial tensile experiments at strain rates from 1 to 32 per second across temperatures from 80 to 110 °C, identifying a strain-hardening transition near a true strain of 1.4 that determines whether further deformation thins the wall uniformly or develops local instabilities [8]. Finite-element extension by Yang, Harkin-Jones, Menary, and Armstrong incorporated non-isothermal viscoelastic behavior and showed that pre-blow timing relative to stretch rod arrival shifts the local strain history by up to 30 percent at constant nominal parameters [9]. Comparison of isothermal and non-isothermal regimes by Woo, Choi, and Lyu against laboratory blow trials on a 500-milliliter carbonated soft drink bottle reported that wall-thickness prediction error rose from 8 percent in the isothermal case to 19 percent when temperature gradients across the preform were ignored [10]. Calibration in those models assumed uniform preform temperature or imposed a shallow linear gradient, leaving wall thicknesses above 5 millimeters outside the validated regime.

Quiescent thermal crystallization in PET differs sharply from strain-induced crystallization, and both contribute to bottle property development. Lu and Hay analyzed isothermal crystallization at temperatures from 110 to 240 °C using differential scanning calorimetry and wide-angle X-ray diffraction, locating the maximum crystal growth rate near 180 °C and showing that primary crystallization completes within 90 seconds at that temperature [6]. Preform

regions held above the glass transition long enough to enter this thermal window before stretching develop spherulitic morphology with reduced biaxial drawability and increased haze [6]. Daver and Demirel modeled preform cooling between injection ejection and the reheat stage, demonstrating that residual thermal history influences the equilibrium crystallinity of the preform feedstock and thereby the temperature window available during subsequent reheating [7]. Once stretching begins, oriented lamellae develop along the principal stretch directions, contributing primarily to hoop strength and burst resistance, with limited effect on vertical Top Load resistance [1]. Venkateswaran, Cameron, and Jabarin further showed that the radial temperature profile at the moment of stretching determines whether the inner and outer wall layers develop similar crystallinity, or whether asymmetric morphology generates differential shrinkage and dimensional drift after demolding [4].

Studies of pre-blow pressure and timing in stretch blow molding have focused on bubble propagation, stretch rod synchronization, and pressure window selection. Salomeia, Menary, and Armstrong instrumented a laboratory-scale rotary machine with miniature pressure transducers and high-speed video to track bubble propagation, identifying three distinct kinematic regimes set by the ratio of pre-blow flow rate to stretch rod velocity [12]. Lontos and Gregoriou applied a similar instrumentation approach to a 1.5-liter geometry and quantified the effect of stretch rod velocity on wall-thickness uniformity, observing a 14 percent reduction in standard deviation when velocity rose from 0.9 to 1.4 meters per second [11]. Lower-bound pressure is limited by the risk of preform contact with the stretch rod, which produces axial drag marks. Upper-bound pressure is limited by premature contact with the mold cavity, which freezes wall thickness before stretch completion. Brandau organizes process recommendations by preform mass, indicating that heavy-format containers operate in the 5 to 9 bar range and require longer pre-blow duration to compensate for inertia [1].

Mechanical evaluation of stretch blown PET containers relies primarily on Top Load resistance, burst pressure, drop impact, and base clearance under load [1]. ASTM D2659 applies a vertical compressive force to the container at a constant displacement rate of 12.5 millimeters per minute, with the maximum force before buckling or panel collapse recorded as the result [14]. For shipping unit loads, ASTM D642 provides a similar protocol at the unit level with provisions for either fixed or swivel platens [15]. Industrial baseline values reported by Brandau range from 80 to 120 kilograms for two-liter beverage bottles and from 150 to 220 kilograms for five-gallon food-grade containers, with significant variation introduced by base design [1]. Inline statistical process control on stretch blow molding lines typically tracks bottle weight, height, and vertical-load resistance on a sampled basis, with control charts updated each shift [1]. Saggin and coworkers indicated that integration of thermal imaging into the existing oven control loop is technically feasible at current camera speeds, though deployment on linear machines has not been reported [13].

Several specific technical questions remain unanswered in the published literature. Absorption-coefficient values used in the Monteix and Cosson models were calibrated against preform walls of 1 to 4 millimeters, and extrapolation to walls of 6 to 8 millimeters has not been independently validated by direct measurement of internal temperature [2, 5]. Strain-rate ranges investigated by Menary and colleagues lie below the effective rates achieved by stretch rods in heavy-format linear equipment, where preform geometry forces longer stretch paths at modestly slower stroke speeds but with higher absolute strain accumulation [8]. No published source links a measured through-thickness temperature differential to a real-time pre-blow trigger setting, leaving operators dependent on empirical lamp-bank tuning and offline product inspection. Heating residence time required to equalize the through-thickness gradient and the resulting cycle-time penalty has not been quantified for preforms exceeding 300 grams. Industrial-scale production data sets supporting finite-element validation

remain sparse for the heavy-format regime, with most available data drawn from laboratory blow rigs [9; 10]. Wall-Gradient Equilibration Protocol addresses several of these questions through a combined offline-calibration and production-line implementation.

Materials and Methods

1. Production environment. Field implementation ran for 24 production weeks (March through August) divided into three intervals: 10 weeks of baseline operation under the existing factory recipe, a two-week transition window with offline calibration trials, and 12 weeks of WGEP deployment. Site was a Ring Container Technologies plant in South Carolina equipped with a SIPA SFL Series six-cavity linear stretch-blow molding system configured for handled large-format containers. Plant operating conditions held ambient temperature at 23 ± 2 °C and relative humidity below 45 percent during the observation window, monitored by the existing building management system.

2. Materials. Preforms were injection molded from food-grade PET resin (intrinsic viscosity 0.83 dl/g, residual acetaldehyde content below 1.5 ppm) sourced from a single domestic supplier under one lot identifier for each ten-thousand-unit batch. Preform geometry included 240 millimeters length, a 38-millimeter neck finish, and 340 ± 4 gram mass. Wall thickness in the body region was 6.4 millimeters, tapering to 4.8 millimeters in the transition zone and 3.2 millimeters at the neck junction. Conditioning before oven entry held the parts at 23 °C ambient for a minimum aging period of 48 hours since injection molding, allowing equilibrium relaxation of residual stresses.

3. Container target. Final containers were 18.9-liter handled food-grade jugs intended for institutional packaging of cooking oil, salad dressing, and bulk sauce products. Container height was 380 millimeters, body diameter 240 millimeters, base diameter 230 millimeters, with an integrated molded handle. Wall thickness specification targeted 0.85 ± 0.10 millimeters in the cylindrical body zone after stretching, with allowable thinning to 0.70 millimeters near the

handle attachment point. Top Load specification required at least 150 kilograms before panel deformation.

4. Equipment configuration. SIPA SFL Series oven length was 4.2 meters with eight independently controlled lamp banks, each containing twelve 3200-watt quartz halogen lamps positioned at radial distances from 38 to 52 millimeters from the preform body axis. Factory baseline configuration grouped the banks into three temperature-control zones. Blowing station capability included a stretch rod with maximum velocity of 1.6 meters per second and a cavity pressure ceiling of 38 bar. Pre-blow circuit was equipped with a proportional flow control valve and a pressure transducer with 0.05-bar resolution feeding the machine programmable logic controller.

5. Offline calibration rig. A laboratory calibration rig was constructed alongside the production line for establishing the correspondence between inline pyrometer reading and internal preform temperature. Three K-type sheathed thermocouples with 0.5-millimeter sheath diameter were inserted into bored cavities at depths of 0.5, 3.0, and 5.5 millimeters from the outer surface of three sacrificial preforms. Each instrumented preform was heated under conditions matched to the production oven, monitored by an Omega DAQ-2416 data logger sampling at 10 hertz, and removed at predetermined dwell times. Surface temperature was simultaneously recorded by a FLIR A655sc thermal imaging camera operating at 0.05 °C sensitivity. A regression curve relating surface pyrometer reading to internal radial gradient was fitted to data from 27 calibration cycles and incorporated into the production oven controller as a lookup table.

6. Production-line instrumentation. During production runs, surface temperature at the oven exit was monitored continuously by an Optris CTlaser 3MH1 infrared pyrometer with spectral range 2.3 micrometers, optimized for PET. Surface temperature mapping at the production line used the FLIR A655sc camera described in subsection 3.5, repositioned at the oven exit with a frame rate of 25 hertz, providing a thermal map of every preform passing on the conveyor.

Post-blow measurement included wall-thickness scanning with an Olympus 38DL Plus ultrasonic gauge equipped with a 10-megahertz dual-element transducer at eight axial positions (50, 100, 150, 200, 250, 300, 340, and 370 millimeters from the base), and Top Load testing on an Instron 5567 universal testing machine in accordance with ASTM D2659 [14]. Center-of-gravity stability was assessed indirectly through the symmetry of the axial wall-thickness profile, as direct gravimetric CG measurement was not available on the production line. Burst pressure was assessed on a sample subset using a SafePack burst tester at a pressurization rate of 1 bar per second.

7. Wall-Gradient Equilibration Protocol parameters. Wall-Gradient Equilibration Protocol configured the oven with a five-zone heating layout interspersed with three convective stabilization gaps. Each stabilization gap consisted of a 0.35-meter conveyor section through which ambient air at 23 °C was directed at 1.2 meters per second toward the preform exterior. Heating-zone power distribution was 65 percent in zones 1 and 2, 80 percent in zones 3 and 4, and 55 percent in zone 5, with the final zone serving to compensate for residual radial gradient before exit. Soak interval after the last lamp bank lasted 24 seconds, during which the preform remained in dark conveyor passage before entering the blowing station. Pre-blow pressure was set to 7.5 bar, triggered at the moment the stretch rod reached 75 percent of its total travel. Main blow pressure was 35 bar. Factory baseline configuration ran 78 seconds of total residence time across three zones without stabilization gaps and fixed pre-blow timing at 60 percent stretch rod travel.

8. Sampling and statistical analysis. Sampling protocol drew thirty containers at random from each production shift, with five shifts per condition and two conditions (baseline and WGEP), for a total of 300 sampled containers. Container-level measurement included eight wall-thickness points, one Top Load value, and selection of every fifth unit for burst pressure testing. Rejection rate was computed from the plant quality management system over the full fourteen-

day production window for each condition, based on total production volume. Sampling subset data supported detailed wall-thickness, Top Load, and burst pressure analysis. Statistical analysis used two-way analysis of variance on wall thickness with condition and axial position as factors, Welch's t-test for paired comparison of Top Load means between conditions, and Cohen's d for effect size. Significance threshold was set at alpha equal to 0.05. Analysis was performed in Minitab 21.

Results

Offline calibration outcomes. Offline calibration trials produced a regression model linking surface pyrometer reading at the oven exit to the internal radial temperature gradient measured between depths 0.5 and 5.5 millimeters. Across 27 calibration cycles spanning oven settings used in subsequent production runs, the relationship was fitted as a second-order polynomial with coefficient of determination R^2 equal to 0.913 and root-mean-square error of 0.84 °C on the held-out validation subset of nine cycles. Polynomial fit identified a surface temperature reading of approximately 108 °C as the operating point at which the measured internal gradient drops below 4 °C, taken as the threshold for stretching with uniform biaxial orientation. Validation runs at the calibration boundary (surface readings between 95 and 115 °C) confirmed the threshold prediction within 0.6 °C of the actual measured gradient, providing the basis for the pre-blow trigger logic implemented during WGEP production runs.

Through-wall temperature gradient under both protocols. Through-wall temperature gradient measured at the oven exit averaged 16.5 ± 1.8 °C under baseline conditions and 4.2 ± 0.7 °C under WGEP (Table 1). Statistical comparison confirmed that the difference is significant at $p < 0.001$ with a large effect size.

Table 1

Through-wall temperature gradient at oven exit under baseline and WGEP protocols (n = 150 preforms per condition)

Condition	Mean ΔT (°C)	SD (°C)	Min (°C)	Max (°C)
Baseline	16.5	1.8	13.1	19.8
WGEP	4.2	0.7	3.0	5.6

Source: author's elaboration

Wall thickness distribution. Wall thickness scanning at eight axial positions revealed a substantial reduction in variability under WGEP without change in mean thickness. Mean wall thickness in the cylindrical body zone remained close to the design target of 0.85 millimeters under both protocols (0.846 ± 0.054 millimeters baseline, 0.851 ± 0.036 millimeters WGEP), consistent with preservation of total stretch ratio. Standard deviation of the wall-thickness profile across the eight axial positions dropped from 0.054 to 0.036 millimeters, a reduction of 33 percent. Two-way analysis of variance returned significant main effects of both condition and axial position, as well as a significant interaction (all $p < 0.001$). Figure 1 presents the axial profile under both protocols; the WGEP profile is markedly tighter in the shoulder transition region (positions 300 to 340 millimeters from the base), where baseline preforms exhibited the greatest variation.

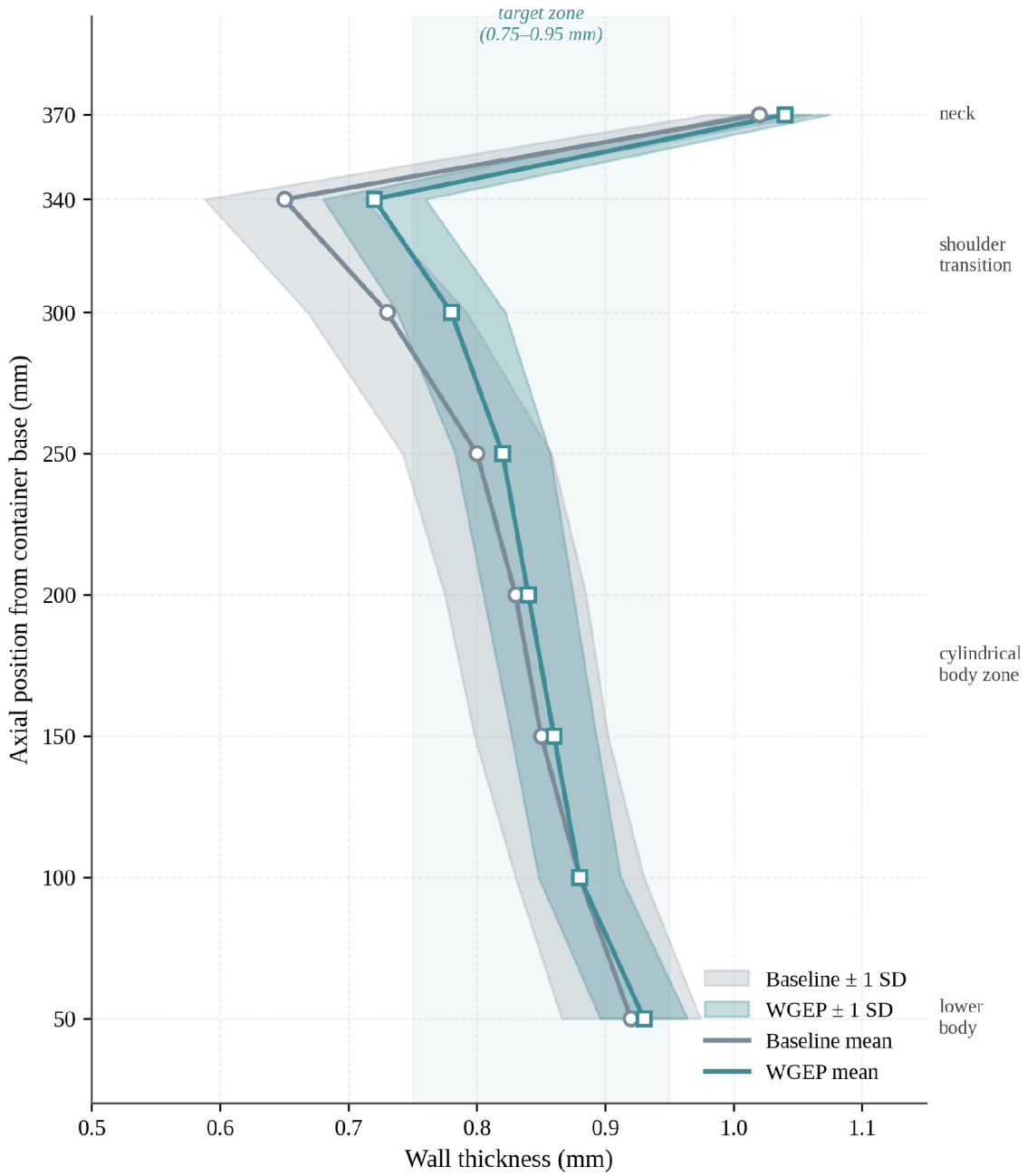


Fig. 1. Axial wall-thickness profile under baseline and WGEP protocols at eight measurement positions (50, 100, 150, 200, 250, 300, 340, 370 millimeters from container base). Shaded bands represent ± 1 SD across n = 150 containers per condition

Source: author's elaboration

Mechanical performance: Top Load and burst pressure. Top Load resistance measured per ASTM D2659 rose from 168.3 ± 8.7 kilograms under baseline conditions to 196.4 ± 6.4 kilograms under WGEP, a relative

improvement of 16.7 percent (Table 2, $p < 0.001$). Burst pressure measured on a one-in-five sampling subset rose from 6.4 ± 0.6 bar to 7.4 ± 0.5 bar, an improvement of 15.6 percent ($p < 0.001$). Failure mode under Top Load testing shifted from base buckling (observed in 78 percent of baseline failures) to panel collapse near the handle insertion point (observed in 64 percent of WGEP failures).

Table 2

Mechanical performance under baseline and WGEP protocols

Metric	Baseline	WGEP	Δ (%)	t	p	Cohen's d
Top Load (kg), mean ± SD	168.3 ± 8.7	196.4 ± 6.4	+16.7	31.6	<0.001	3.7
Burst pressure (bar), mean ± SD	6.4 ± 0.6	7.4 ± 0.5	+15.6	7.0	<0.001	1.8

Source: author's elaboration

*Top Load: n = 150 per condition. Burst pressure: n = 30 per condition

Production-line outcomes: rejection rate and cycle time. Rejection rate during the fourteen-day production windows fell from 1.4 percent under baseline conditions to 0.5 percent under WGEP, with the absolute reduction representing close to 86 fewer rejected containers per shift at the plant's typical output of 9,500 units per shift. WGEP rejection rate stabilized within the first three production days after deployment and remained flat thereafter, while baseline rejection fluctuated between 1.2 and 1.7 percent across the fourteen-day window without a discernible trend. Cycle-time analysis confirmed an average penalty of 2.4 seconds per cavity per cycle, distributed across the three stabilization gaps and the extended soak interval. Effective throughput dropped from 1,520 containers per hour under baseline to 1,473 containers per hour under WGEP, a reduction of 3.1 percent. Aggregated across the production window, this trade-off corresponded to 3,790 fewer produced containers per week, paired with 28,500 fewer rejected containers per week, yielding a net favorable balance of around 24,700 saleable containers per week.

Validation of WGEP gradient threshold and Top Load linkage. Segmenting the 300 sampled containers by measured ΔT at the moment of stretching produced a near-monotonic relationship between gradient and Top Load resistance (Figure 2): containers with ΔT below 4 °C exhibited Top Load of 198.1 ± 5.9 kilograms, those with ΔT between 4 and 8 °C exhibited 187.4 ± 7.2 kilograms, and those with ΔT above 8 °C exhibited 169.8 ± 9.4 kilograms. Linear regression of Top Load against ΔT returned a slope of −2.4 kilograms per degree Celsius ($R^2 = 0.82$, $p < 0.001$). The 4 °C threshold incorporated into WGEP represents the engineering specification at which Top Load consistently meets customer requirements above 196 kilograms; further reduction would require disproportionate increases in residence time and energy consumption.

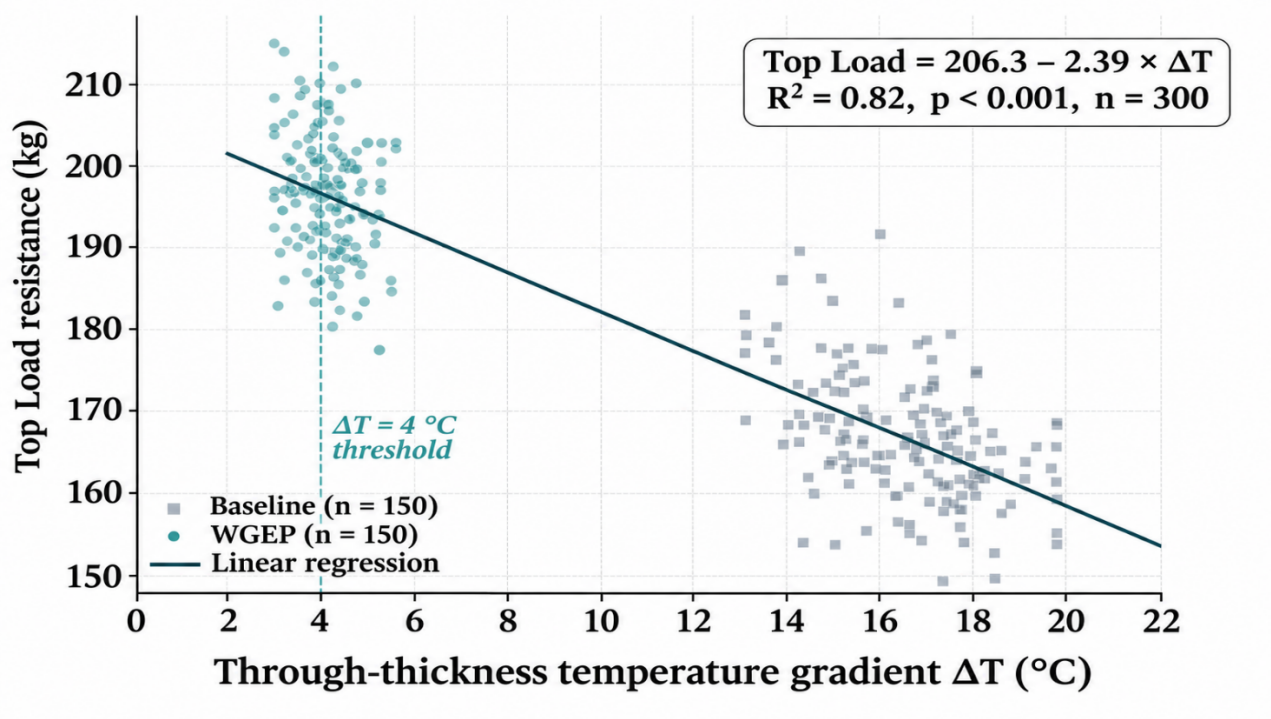


Fig. 2. Linear regression of Top Load resistance against measured through-thickness temperature gradient (ΔT) at the moment of stretching, n = 300 sampled containers. Vertical dashed line marks the ΔT = 4 °C threshold incorporated into WGEP pre-blow trigger logic

Source: author's elaboration

Discussion. Reduction of through-wall temperature gradient under WGEP can be attributed to two coupled mechanisms operating during the stabilization gaps and soak intervals. Convective cooling of the outer surface during each gap lowers the skin temperature while internal conduction continues to transport absorbed infrared energy toward the core. Monteix and colleagues predicted this nonlinear energy accumulation near the outer surface for walls below 4 millimeters [2]; at 6.4 millimeters the effect intensifies, and the stabilization gaps serve to interrupt it before outer-skin crystallization onset. By the time the preform enters the next heating zone, the radial profile has partially flattened, and the subsequent lamp exposure raises both surfaces more uniformly than a single uninterrupted pass would achieve.

Improvement in wall-thickness uniformity follows directly from gradient reduction. When the inner and outer preform surfaces reach the stretching station at similar temperatures, the viscosity difference between them narrows, and the stretch rod encounters a more mechanically homogeneous tube. Under baseline conditions, the cooler inner surface crossed the strain-hardening threshold [8] earlier than the warmer outer surface, producing the asymmetric thickness pattern visible in the shoulder transition region of Figure 1. Under WGEP, both surfaces entered the strain-hardening regime within a narrower strain increment, and the resulting profile converged because differential thinning across the shoulder transition geometry was eliminated.

Shift in failure mode from base buckling to handle-region panel collapse has practical significance. Improved base orientation under WGEP indicates that the cooler inner surface under baseline conditions failed to develop sufficient strain-induced lamellae during the final stages of blowing. Once the gradient was equalized, the failure locus migrated to the handle insertion point, a geometric stress concentrator independent of the heating protocol. Addressing this new limiting feature would require mold-design modification or localized material redistribution during injection molding of the preform.

Regression between through-thickness gradient and Top Load resistance (subsection 4.6) provides a quantitative planning tool for operators of linear stretch-blow equipment. To the author's knowledge, no prior peer-reviewed work has linked a measured gradient value to a specific mechanical outcome at production scale; published work has established qualitatively that radial temperature asymmetry degrades container properties [4] and that pre-blow timing mismatch accumulates into measurable strain-history shifts [9]. The regression equation allows an operator to estimate the mechanical penalty associated with a specific gradient excursion and to set process alarm limits accordingly.

Cycle-time penalty imposed by the stabilization gaps and extended soak represents a modest throughput reduction that is more than offset by the rejection-rate improvement. Net weekly output gain exceeded six times the throughput loss, confirming that the trade-off is favorable at output rates typical of large-format linear equipment. Production environments with preform mass below 200 grams and cycle times under 60 seconds are unlikely to benefit from the stabilization-gap architecture, as thinner walls equalize naturally during standard oven residence.

Several limitations qualify the reported findings. Single-site implementation means that variation in ambient conditions, resin supply, and machine wear patterns across other facilities could shift the magnitude of improvements. Regression was fitted on pooled data from two process conditions occupying opposite ends of the gradient range; additional data from partially optimized configurations would strengthen confidence in linearity. Seasonal variation in ambient temperature from March to August at the South Carolina site may have introduced a slow drift that the current analysis does not separate from the protocol effect. Center-of-gravity position was not measured directly; the indirect assessment through wall-thickness symmetry captures material distribution

without accounting for density gradients arising from differential crystallinity across the container wall.

Conclusions. Wall-Gradient Equilibration Protocol demonstrated that through-thickness temperature management is both achievable and economically justified on linear stretch-blow equipment processing thick-wall preforms for large-format PET containers.

Interspersing convective stabilization gaps within the infrared oven and adding a post-heating soak interval brought the radial temperature gradient within the design target without requiring hardware modification beyond oven-zone reconfiguration, making the protocol transferable to other linear stretch-blow platforms with independently controlled lamp banks.

Coupling pre-blow timing to the measured gradient state through a pyrometer-based lookup table proved operationally stable across a full production campaign, requiring no intervention from the machine programmable logic controller beyond a single parameter table upload.

Mechanical performance of the finished container improved across all tested metrics, with the dominant failure mode shifting from a heating-related defect (base buckling) to a geometry-related constraint (handle-insertion stress concentration), indicating that the protocol effectively eliminates the thermal contribution to container weakness.

Throughput penalty imposed by the extended heating sequence was more than offset by rejection-rate reduction, producing a favorable net output balance applicable to any large-format linear operation where quality losses currently exceed the single-digit percentage range.

Regression linking through-thickness gradient to vertical compressive resistance provides process engineers with a quantitative planning tool for setting alarm limits, evaluating equipment upgrades, and benchmarking oven performance across production campaigns on comparable linear stretch-blow equipment.

Future work should extend the calibration model to seasonal ambient temperature variation and lamp degradation over campaigns exceeding six months. Collection of intermediate-gradient data would validate linearity across the full operating range. Integration of closed-loop feedback from an inline thermal imaging system could replace the current open-loop lookup table with real-time adaptive control, enabling fully automated gradient management without operator intervention at the batch-change level.

References

1. Brandau O. (2017). Stretch Blow Molding (3rd ed.). William Andrew Publishing. ISBN 9780323510172.

2. Monteix S., Schmidt F., Le Maoult Y., Ben Yedder R., Diraddo R.W., Laroche D. (2001). Experimental study and numerical simulation of preform or sheet exposed to infrared radiative heating. *Journal of Materials Processing Technology, 119,* 90–97. DOI: 10.1016/S0924-0136(01)00882-2.

3. Schmidt F.M., Agassant J.F., Bellet M. (1998). Experimental study and numerical simulation of the injection stretch/blow molding process. *Polymer Engineering and Science, 38*(9), 1399–1412. DOI: 10.1002/pen.10310.

4. Venkateswaran G., Cameron M.R., Jabarin S.A. (1998). Effects of temperature profiles through preform thickness on the properties of reheat-blown PET containers. *Advances in Polymer Technology, 17*(3), 237–249.

5. Cosson B., Schmidt F., Le Maoult Y., Bordival M. (2011). Infrared heating stage simulation of semi-transparent media using ray tracing method. *International Journal of Material Forming, 4,* 1–10. DOI: 10.1007/s12289-010-0985-8.

6. Lu X.F., Hay J.N. (2001). Isothermal crystallization kinetics and melting behaviour of poly(ethylene terephthalate). *Polymer, 42*(21), 9423–9431. DOI: 10.1016/S0032-3861(01)00502-X.

7. Daver F., Demirel B. (2012). A simulation study of the effect of preform cooling time in injection stretch blow molding. *Journal of Materials Processing Technology, 212(*11), 2400–2405. DOI: 10.1016/j.jmatprotec.2012.06.004.

8. Menary G.H., Tan C.W., Harkin-Jones E.M.A., Armstrong C.G., Martin P.J. (2012). Biaxial deformation and experimental study of PET at conditions applicable to stretch blow molding. *Polymer Engineering and Science, 52*(3), 671–688. DOI: 10.1002/pen.22134.

9. Yang Z.J., Harkin-Jones E., Menary G.H., Armstrong C.G. (2004). A non-isothermal finite element model for injection stretch-blow molding of PET bottles with parametric studies. *Polymer Engineering and Science, 44,* 1379–1390. DOI: 10.1002/pen.20133.

10. Woo I.Y., Choi D.-H., Lyu M.-Y. (2024). Isothermal and non-isothermal computer simulation of a stretch blow molding process and comparison with experiments. *Journal of Reinforced Plastics and Composites.* DOI: 10.1177/07316844231198687.

11. Lontos A., Gregoriou A. (2019). The effect of the deformation rate on the wall thickness of 1.5LT PET bottle during ISBM process. *Procedia CIRP, 81,* 1307–1312. DOI: 10.1016/j.procir.2019.04.018.

12. Salomeia Y.M., Menary G.H., Armstrong C.G. (2013). Experimental Investigation of Stretch Blow Molding, Part 2. *Advances in Polymer Technology, 32*(S1), E436–E450. DOI: 10.1002/adv.21291.

13. Saggin B., Tarabini M., Scaccabarozzi D., Cornolti L., Giberti H., Moschioni G. (2019). Non-contact measurement of the temperature profile of PET preforms. *Measurement, 133,* 412–420. DOI: 10.1016/j.measurement.2018.10.044.

14. ASTM D2659-16. Standard Test Method for Column Crush Properties of Blown Thermoplastic Containers. ASTM International, West Conshohocken, PA, 2016.

15. ASTM D642-20. Standard Test Method for Determining Compressive Resistance of Shipping Containers, Components, and Unit Loads. ASTM International, West Conshohocken, PA, 2020.